Audio Engineering Society

Convention Paper 10657

Presented at the 154th Convention
2023 May 13–15, Espoo, Helsinki, Finland

This paper was peer-reviewed as a complete manuscript for presentation at this convention. This paper is available in the AES E-Library (http://www.aes.org/e-lib), all rights reserved. Reproduction of this paper, or any portion thereof, is not permitted without direct permission from the Journal of the Audio Engineering Society.

Sound spectrum modulation generated by circularly moving sound sources

Timothy Schmele[1,2] and Adán Garriga[1]

[1]*Eurecat, Centre Tecnològic de Catalunya, Tecnologies Multimèdia, Barcelona, 08005, Spain*
[2]*Institut für Musikinformatik und Musikwissenschaft (IMWI), Hochschule für Musik, Karlsruhe, Germany*

Correspondence should be addressed to Timothy Schmele (tim.schmele@eurecat.org)

ABSTRACT

This paper presents the phenomenon in which circularly rotating sound sources exhibit a spectral split at the center of rotation. It is shown that this spectral split occurs exclusively in the velocity field and is equivalent to the angular speed of the rotation. However, it does not affect the pressure field at the point of measurement, showing no change to the emitted spectrum of the source. To test this in both 2D and 3D, the sound field of a rapidly rotating sound source is reconstructed using Wavefield Synthesis. The reconstruction is done as faithfully as possible by minimising the discretisation artifacts using a large number of secondary sources along the circle perimeter and sphere surface respectively. The measurements taken confirm the theoretical findings. The applications of this phenomenon can range from fault analysis of rotating machines to spatial audio and may also inform on the perception of rotating sound beyond the previously determined limit.

1 Introduction

Physical effects produced by moving sound sources have been reported since the demonstration of the Doppler effect in sound [1] and became relevant in many fields such as ultrasound for medical diagnosis [2], underwater communications [3], gesture detection [4] or virtual sound rendering [5]. In fact, phenomena like the Doppler effect should be included in sound rendering in virtual environments to not lose immersion due to fast moving sound sources [6].

Apart from the Doppler effect caused by linearly moving sounds, little investigation has gone into the spectral effects caused by high speeds of circularly moving sounds. As a matter of fact, few objects in the natural world rotate fast enough to cause noticeable spectral distortions and it has also been shown that our ability to follow a sound circling around us breaks down at about 3 rotations per second [7]. Most famously in the music world, the well-known Leslie loudspeaker features a fast rotating horn and baffle. However, with the receiver being located outside the center of rotation, it mostly makes use of a modulated Doppler effect to achieve an effect akin to tremolo [8]. But when we think about other applications such as fault diagnosis of rotating machines [9] (a critical subject in the automobile industry), or sound synthesis in the context of spatial audio [10], the spectral change of sounds due to circularly moving sound sources can play an important role.

In the present paper, we will consider harmonic sound sources moving on a ring (2D case) and on the surface of a sphere (3D case). We will show that sound sources circularly moving at high velocities produce secondary

effects in the velocity field leading to the generation of harmonics in the sound spectrum, while not affecting the pressure field at all. These effects are due to the interplay between the frequency of the sound source and the angular velocity of the sound source through space.

2 Circularly moving harmonic sound source

Let's consider a harmonic point source, where the acoustic pressure, p_{rad}, radiated from the sound source is given by:

$$p_{\text{rad}}(t) = A\cos(\omega_s t + \phi) \,, \tag{1}$$

where A is the amplitude, ω_s is the angular frequency of the oscillation and ϕ is the initial phase. This harmonic perturbation generates pressure and velocity waves, which follow Euler's equations [11, p. 243]:

$$\frac{\partial p}{\partial t} + \rho c^2 \left[\frac{\partial v_x}{\partial x} + \frac{\partial v_y}{\partial y}\right] = 0 \,, \tag{2}$$

$$\rho \frac{\partial v_x}{\partial t} + \frac{\partial p}{\partial x} = 0 \,, \tag{3}$$

$$\rho \frac{\partial v_y}{\partial t} + \frac{\partial p}{\partial y} = 0 \,, \tag{4}$$

$$\rho \frac{\partial v_z}{\partial t} + \frac{\partial p}{\partial z} = 0 \,, \tag{5}$$

where ρ is the density of the fluid and c is the speed of sound inside this fluid. The velocity vector of the molecules of the fluid is given by $\mathbf{v} = (v_x, v_y, v_z)$ and p is the pressure relative to a given pressure reference level (usually the atmospheric pressure). The first Euler equation (2) states that a velocity divergence produces a compression of the fluid, while the remaining equations (3)-(5) state that a pressure gradient produces an acceleration of the fluid. These equations are valid for small velocities and small values of the relative pressure.

In the following subsections, we shall let this harmonic sound source rotate around a center position in a free field. In particular, we shall investigate the secondary effects caused by a circularly moving sound source on both a ring in a plane, as well the surface of a sphere.

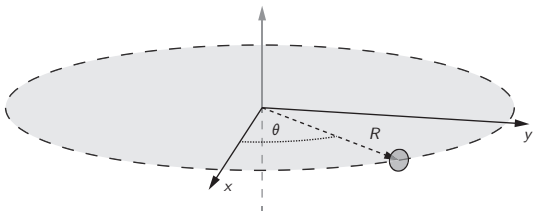

Fig. 1: Sound source on a ring of radius R, θ being the angular coordinate.

2.1 Harmonic sound source on a ring

Consider a harmonic sound source moving along a ring of radius $R > 0$ (see Figure 1). In 2D, we must first restrict our velocity vector to a plane: $\mathbf{v} = (v_x, v_y)$. Considering equations (2)-(4), the acoustic field generated at the centre of the ring by the harmonic point source (equation (1)), located at an azimuth angle θ in the ring (see Figure 1) is then given by:

$$p_{\text{centre}}(t) = A'\cos(\omega_s t + \phi') \,, \tag{6}$$

$$v_{x_{\text{centre}}}(t) = \frac{A'}{c\rho}\cos(\omega_s t + \phi')\cos\theta \,, \tag{7}$$

$$v_{y_{\text{centre}}}(t) = \frac{A'}{c\rho}\cos(\omega_s t + \phi')\sin\theta \,, \tag{8}$$

where $A' < A$ is the amplitude after geometrical and physical attenuation (assuming an isotropic medium), ω_s is the angular frequency of the radiated sound, c is the speed of sound, ρ is the density of the medium and $\phi' = \phi + k_s R$, k_s being the wavenumber, which is related to the angular frequency by the dispersion relation, $k_s = \frac{\omega_s}{c}$. Without loss of generality, we shall consider $\phi' = 0$ from now on.

If the sound source moves along the ring following some trajectory $\theta(t)$, the acoustic field generated at the centre is simply given by:

$$p_{\text{centre}}(t) = A'\cos(\omega_s t) \,, \tag{9}$$

$$v_{x_{\text{centre}}}(t) = \frac{A'}{c\rho}\cos(\omega_s t)\cos\theta(t) \,, \tag{10}$$

$$v_{y_{\text{centre}}}(t) = \frac{A'}{c\rho}\cos(\omega_s t)\sin\theta(t) \,. \tag{11}$$

Let's now consider the particular case in which the sound source travels along the ring at a constant angular

speed ω_r, i.e. $\theta(t) = \omega_r t$. Substituting in equations (9)-(11) and arranging in simple harmonic terms we get:

$$p_{\text{centre}}(t) = A' \cos(\omega_s t) \ , \tag{12}$$

$$v_{x_{\text{centre}}}(t) = \frac{A'}{2c\rho}\Big[\cos((\omega_s+\omega_r)t) + \cos((\omega_s-\omega_r)t)\Big] \ , \tag{13}$$

$$v_{y_{\text{centre}}}(t) = \frac{A'}{2c\rho}\Big[\sin((\omega_s+\omega_r)t) - \sin((\omega_s-\omega_r)t)\Big] \ . \tag{14}$$

Equations (12)-(14) show that a moving sound source on a ring generates two sidebands in the velocity field at the centre of the ring ($\omega_s - \omega_r$ and $\omega_s + \omega_r$) on top of the periodic acoustic pressure signal. Therefore, the movement of the source at constant speed modulates the amplitude of the velocity components while maintaining the periodicity of the pressure due to the fact that the sound source is always at the same distance from the centre.

2.2 Harmonic sound source on a sphere

We shall now add the acceleration along the z-axis (5). Thus, our velocity vector is now three-dimensional: $\mathbf{v} = (v_x, v_y, v_z)$, and, consequentially, we receive a slightly modified set of equations for the acoustic field at the centre of the ring, generated by the harmonic point source in equation (1), and located at an azimuth angle ϕ and elevation angle θ (see Figure 2):

$$p_{\text{centre}}(t) = A' \cos(\omega_s t) \ , \tag{15}$$

$$v_{x_{\text{centre}}}(t) = \frac{A'}{c\rho}\cos(\omega_s t)\sin\theta\cos\phi \ , \tag{16}$$

$$v_{y_{\text{centre}}}(t) = \frac{A'}{c\rho}\cos(\omega_s t)\sin\theta\sin\phi \ , \tag{17}$$

$$v_{y_{\text{centre}}}(t) = \frac{A'}{c\rho}\cos(\omega_s t)\cos\theta \ , \tag{18}$$

To illustrate the spectrum produced by the rotation in two dimensions, let's now consider a particular trajectory where the two spherical angles change linearly with time, i.e. $\theta(t) = \omega_{r1} t$ and $\phi(t) = \omega_{r2} t$. The acoustic field generated by the harmonic sound source from

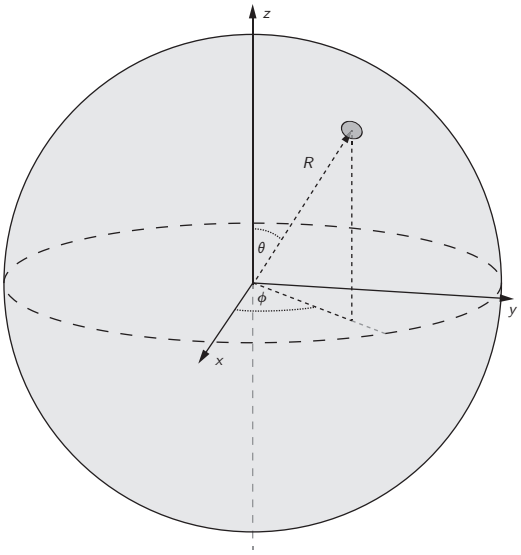

Fig. 2: Sound source on the surface of a sphere of radius R. θ is the elevation angle and ϕ is the azimuth angle.

equation (1) at the centre of the sphere is given by equations (15)-(18), which, in harmonic terms, can be rewritten:

$$p_{\text{centre}}(t) = A' \cos(\omega_s t) \ , \tag{19}$$

$$v_{x_{\text{centre}}}(t) = \frac{A'}{4c\rho}\Big[\sin((\omega_s+\omega_{r1}-\omega_{r2})t) - \sin((\omega_s-\omega_{r1}+\omega_{r2})t) + \sin((\omega_s+\omega_{r1}+\omega_{r2})t) - \sin((\omega_s-\omega_{r1}-\omega_{r2})t)\Big], \tag{20}$$

$$v_{y_{\text{centre}}}(t) = \frac{A'}{4c\rho}\Big[\cos((\omega_s-\omega_{r1}+\omega_{r2})t) + \cos((\omega_s+\omega_{r1}+\omega_{r2})t) - \cos((\omega_s-\omega_{r1}-\omega_{r2})t) - \cos((\omega_s+\omega_{r1}+\omega_{r2})t)\Big], \tag{21}$$

$$v_{z_{\text{centre}}}(t) = \frac{A'}{2c\rho}\Big[\cos((\omega_s+\omega_{r1})t) + \cos((\omega_s-\omega_{r1})t)\Big] \ . \tag{22}$$

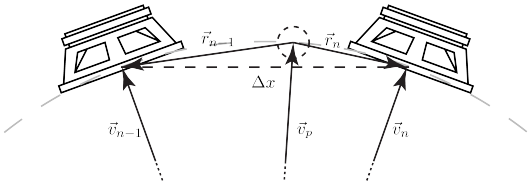

Fig. 3: Depiction of a sound source between two secondary sources, visualised by drivers.

Therefore, this particular trajectory of the sound source, $(\theta(t) = \omega_{r1}t, \phi(t) = \omega_{r2}t)$, generates six sidebands in the velocity field:

$$\begin{aligned}
\omega_1 &= \omega_s + \omega_{r1} + \omega_{r2} \ , \\
\omega_2 &= \omega_s + \omega_{r1} - \omega_{r2} \ , \\
\omega_3 &= \omega_s - \omega_{r1} + \omega_{r2} \ , \\
\omega_4 &= \omega_s - \omega_{r1} - \omega_{r2} \ , \\
\omega_5 &= \omega_s + \omega_{r1} \ , \\
\omega_6 &= \omega_s - \omega_{r1} \ .
\end{aligned} \tag{23}$$

3 Simulations

To test the theoretical findings, we rendered the moving sound source using Wavefield Synthesis (WFS) in anechoic conditions. In essence, WFS provides a discretised solution to the Kirchhoff-Helmholtz integral for convex volumes by means of secondary sources along the volume's perimeter [12, 13]. Each secondary source n is driven by the driving function [10]:

$$s_n(t) = C(f)\frac{\cos\theta_n}{|\vec{r}_n|}e^{-jwr_n}s(t), \tag{24}$$

where $\vec{r}_n$ is the vector pointing from the secondary source n to the virtual sound source, the angle θ_n describes the angular distance between the virtual sound source and the secondary source n and $C(f)$ is a frequency dependent constant.

For the purpose of this analysis, we shall let the virtual source move on a circle of radius r, along which N secondary sources are equally distributed. However, equation (24) exhibits that, as the virtual sound source travels along the perimeter and approaches a secondary source n, it is equally decreased in amplitude by $\cos\theta_n$, as θ_n tends towards 90°, and increased in amplitude as the distance $|\vec{r}_n|$ tends towards 0 (see Figure 3).

A solution to this conundrum is to define a threshold using the regular distance between two secondary sources Δx beyond which $|\vec{r}_n|$ may not decrease anymore. Additionally, the term θ_n is then replaced with a term for the gain coefficient g_n. This results in a type of "pair-wise panning" between the closest secondary sources $n-1$ and n [14]:

$$g_{n-1} = \frac{|\vec{r}_n|}{|\vec{r}_{n-1}| + |\vec{r}_n|}, \quad g_n = \frac{|\vec{r}_{n-1}|}{|\vec{r}_{n-1}| + |\vec{r}_n|}. \tag{25}$$

3.1 Planar Movement

To measure the pressure and pressure gradient in a plane we implemented a first order Ambisonic microphone [15, 16] at the center of the ring. In 2D, this can be done by superimposing an omni-directional polar pattern over two figure-eight polar patterns perpendicular to each other (see Figure 4), giving us a total of 3 output signals:

$$m_p(t) = \sum_{i=0}^{N} s_i(t) \ , \tag{26}$$

$$m_x(t) = \frac{1}{c\rho}\sum_{i=0}^{N} s_i(t)\cos(\bar{\theta}i) \ , \tag{27}$$

$$m_y(t) = \frac{1}{c\rho}\sum_{i=0}^{N} s_i(t)\sin(\bar{\theta}i) \ , \tag{28}$$

where $s_i(t)$ is the signal generated by the driving function for the i-th secondary source and $\bar{\theta} = 2\pi/N$ is the regular angular distance between any two neighboring secondary sources (see Figure 4).

Figure 5 shows the DFT magnitude analysis of the three output audio streams $m_p(t)$, $m_x(t)$ and $m_y(t)$ from circularly moving a virtual sound source at $1kHz$ at a distance of $r = 1m$ while emitting a pilot tone of $5kHz$ at the same time. Discretising the circle's perimeter results in unwanted aliasing effects, like in the case of linear arrays of secondary sources [17]. However, unlike the linear case, to which, given the regular distance between secondary sources Δx, a frequency limit can be determined below which spatial aliasing can be avoided, it has been shown that in the circular case no anti-aliasing condition can applied in general [17]. Thus, to merely minimise these artifacts, we chose a relatively high number of 1000 secondary sources, resulting in $\bar{\theta} = 0.36^\circ$.

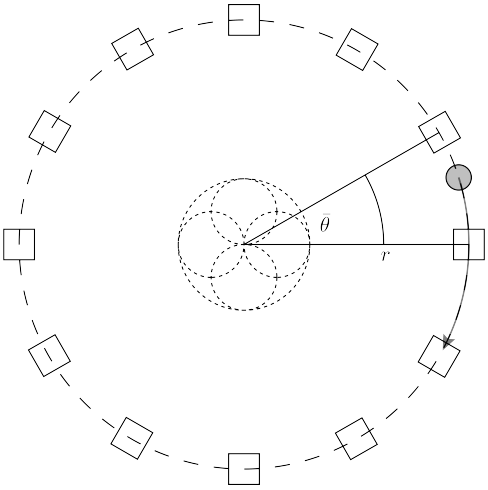

Fig. 4: An illustration of the simulation setup. The virtual sound source, represented by a translucent circle, is rendered using the secondary sources as represented by squares. In the center sits the Ambisonic microphone, represented by it's three polar patterns. It should be noted, that the number of secondary sources is only illustrative and that the secondary sources are all considered monopoles.

It can be seen in Figure 5 that the signals from all secondary sources sum up in the pressure field $m_p(t)$ and result in the original pilot tone of $5kHz$. It is known that moving a virtual sound source through a circular multichannel loudspeaker array causes artifacts to appear in each individual loudspeaker [10]. However, $m_p(t)$ in Figure 5 demonstrates that these artifacts cancel each other out if measured in the exact center of the rotation.

More importantly, $m_x(t)$ and $m_y(t)$ in Figure 5 demonstrate that the pilot tone is split by the sum and difference of the angular velocity of $1kHz$, resulting in $4kHz$ and $6kHz$ respectively. For these measurements, we have chosen $c = 340m/s$ and $\rho = 1.225kg/m^3$ at $15C^\circ$ respectively. The measured magnitude difference between frequencies found in $m_p(t)$ and $m_x(t)$ or $m_y(t)$ is therefore around $-58.4dB$, which complies with the theoretical findings:

$$20\log\left(\frac{1}{2c\rho}\right) = -58.4\ dB \tag{29}$$

3.2 Spherical Movement

In order to extrapolate this technique to a sphere, we created a two layer WFS technique. The first layer represents the planar ring, along which the virtual sound source is rotated around, just like in the previous 2D case. This first layer itself is then virtualised, meaning that its secondary sources are treated like virtual sound sources in the second layer. Each virtual secondary source of the first layer is thus rendered along a respective, corresponding ring of secondary sources in the second layer. It should be noted that equations (26)-(28) only depend on the angle between the monopole secondary sources and not the euclidian distance between each other or the source. If viewed together, all rings of secondary sources in the second layer then form a sphere (see Figure 6). The circular movement of the sound source around the virtual ring of the first layer then constitutes one spherical dimension (e.g. θ), whereas the rotation of the entire ring of the first layer through the second layer constitutes the second (e.g. ϕ).

For simplicity, we shall choose the same amount of secondary sources N in the first layer, as well as each ring of the second, meaning that the same regular angular distance $\bar{\theta}$ applies to all. Also, we shall *not* try to optimise and reuse existing rings in the second layer

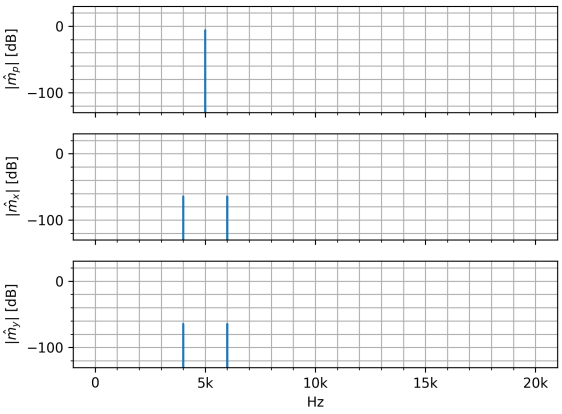

Fig. 5: Magnitude results of rendering a virtual sound source moving along a circle at an angular velocity of $1kHz$ while emitting a $5kHz$ pilot tone using 1000 secondary sources along the rotation perimeter.

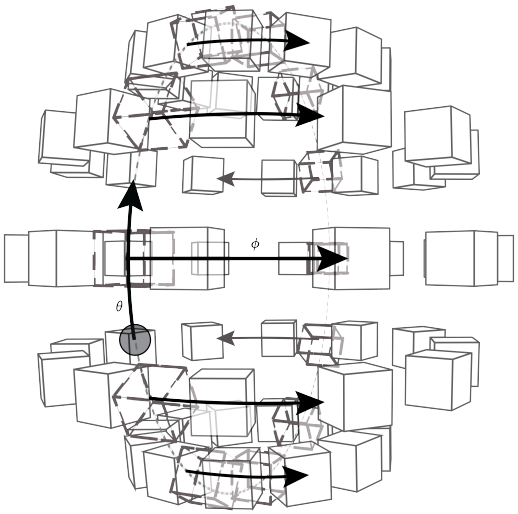

Fig. 6: Example sketch of how the two layered WFS system is built. The sound source is represented by the translucent circle. It is rendered through the first layer of virtual secondary sources, represented by dashed, darker cubes. Each virtual secondary source is rendered by a corresponding ring of secondary sources in the second layer (lighter cubes), which is oriented to be perpendicular to the orientation of the ring in the first layer. Oriented as shown here, the virtual sound source's circular movement through the first layer constitutes its movement in elevation (θ), while the rotation of the entire ring of the first layer through the second layer constitutes the azimuth movement of the source (ϕ). The amount of secondary sources in each ring is just illustrative and each secondary source should be considered a monopole. Also, consider that some rings in the second layer may overlap.

for virtual secondary sources in the first layer where it could be appropriate. While this does mean that rings in the second layer may perfectly overlap, this does not constitute an issue in the final rendering. The signal $s_{ij}(t)$ is then a combination of the driving function for the i-th secondary source in the first layer and the j-th secondary source in the i-th ring of the second layer. A first order Ambisonic microphone in 3D can be constructed by adding a third, orthogonal figure-eight polar pattern to the superposition already done in equations (26)-(28) giving us four audio streams of output [15, 16]:

$$m_p(t) = \sum_{i,j=0}^{N} s_{ij}(t) \ , \tag{30}$$

$$m_x(t) = \frac{1}{c\rho} \sum_{i,j=0}^{N} s_{ij}(t) \sin(\bar{\theta} i) \cos(\bar{\theta} j) \ , \tag{31}$$

$$m_y(t) = \frac{1}{c\rho} \sum_{i,j=0}^{N} s_{ij}(t) \sin(\bar{\theta} i) \sin(\bar{\theta} j) \ , \tag{32}$$

$$m_z(t) = \frac{1}{c\rho} \sum_{i,j=0}^{N} s_{ij}(t) \cos(\bar{\theta} i) \ . \tag{33}$$

In Figure 7 the DFT magnitude analysis of the microphone channels $m_p(t)$, $m_x(t)$, $m_y(t)$ and $m_z(t)$ of a sound source emitting a pilot tone of $5kHz$ while circularly moving the source at an angular velocity of $1kHz$ vertically and $500Hz$ horizontally on the surface of a sphere with $r = 1m$ is shown. As in the 2D case, we opted to use 1000 secondary sources, both in the first layer, as well as each ring of the second, resulting in $\bar{\theta} = 0.36°$ in each case.

Again, the pressure field yields the pilot tone $5kHz$. In accordance with equation (23), we can observe the

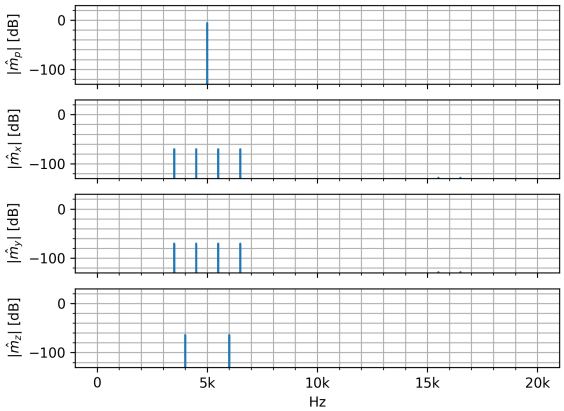

Fig. 7: Magnitude results of rendering a virtual sound source moving on a sphere with an angular velocity of $1kHz$ vertically and $500Hz$ horizontally, while emitting a $5kHz$ pilot tone using 1000 secondary sources along the rotation perimeter.

sum and difference frequencies between the pilot tone and vertical angular velocity, $4kHz$ and $6kHz$, in the vertical velocity component $m_z(t)$. Furthermore, we can observe a second frequency split in $m_x(t)$ and $m_y(t)$, splitting the frequency content observed in $m_z(t)$ by the horizontal angular velocity, resulting in $3.5kHz$, $4.5kHz$, $5.5kHz$ and $6.5kHz$ respectively.

Considering that $c = 340m/s$ and $\rho = 1.225kg/m^3$ at 15C$^\circ$, we can measure a magnitude difference of $-58.4dB$ between the frequencies observed in $m_p(t)$ and $m_z(t)$, as well as $-64.5dB$ between those observed in $m_p(t)$ and $m_x(t)$ or $m_y(t)$ respectively, which complies with the theoretical findings once more.

4 Summary

In this paper we have studied spectral effects of fast circularly moving sound sources. Specifically, we looked at the secondary effects caused by moving a sound source both along a circle in 2D and on a sphere in 3D.

In the 2D case, it has been shown that a spectrum split occurs in the velocity field using constant angular velocities. Moreover, because the pressure component maintains the input signal, it can be said that the spectral result in the acoustic field is comparable to Amplitude Modulation synthesis [18]. The generalization to the 3D case is straightforward and leads to more complex spectra. In section 2.2 we have shown, as an example, that a trajectory, where the two angular variables change linearly with time, leads to the generation of six harmonics on top of the frequency of the sound source.

The theoretical findings were tested using simulations. Using Wavefield Synthesis the acoustic field of a circularly moving sound source at high angular velocities can be reconstructed and measured with a velocity probe, such as an Ambisonics microphone. The results comply with the theoretical findings. The high number of secondary sources was chosen to minimise the artifacts generated by the circle's discretisation, while also representing a trade-off against computational complexity. Future work will need to investigate the interactions between spatial aliasing and the effects described here to reduce the number of secondary sources to a more realistic number.

The present paper shows a physics phenomenon of circularly moving sound sources which has not been reported before (up to the authors' knowledge). As was mentioned in the introduction, this phenomenon can potentially be used for different applications such as to detect faults in rotating engines. Furthermore, the authors plan to use this phenomenon as a basis to develop new spatial sound synthesis approaches. Spatial sound synthesis refers to sound synthesis techniques that include spatial parameters in the sound creation process [10, 19, 20, 21, 22].

Additionally, the spectral split shown here may also point towards a mechanism that can allow a human listener to perceive a circularly moving sound source above the previously determined limit of 3Hz [7], by switching the perceptual mode from following the source to following the spectral distortion. Future work thus includes investigating the perceptual implications of these findings.

References

[1] Buys Ballot, C. H. D., "Akustische Versuche auf der Niederlandische Eisenbahn, nebst gelegentliche Bemerkungen zur Theorie des Herrn Prof. Dobbler," *Annalen der Physik und Chemie*, 66, pp. 321–351, 1845, doi: https://doi.org/10.1002/andp.18451421102.

[2] Routh, H. F., "Doppler ultrasound," *IEEE Engineering in Medicine and Biology Magazine*, 15(6), pp. 31–40, 1996, doi: https://doi.org/10.1109/51.544510.

[3] Johnson, M., Freitag, L., and Stojanovic, M., "Improved Doppler tracking and correction for underwater acoustic communications," in *1997 IEEE International Conference on Acoustics, Speech, and Signal Processing*, pp. 575–578, IEEE, 1997, doi: https://doi.org/10.1109/ICASSP.1997.599703.

[4] Gupta et al., S., "Soundwave: using the doppler effect to sense gestures," in *Proceedings of the SIGCHI Conference on Human Factors in Computing Systems*, pp. 1911–1914, ACM, 2008, doi: https://doi.org/10.1145/2207676.2208331.

[5] Ahrens, J. and Spors, S., "Reproduction of moving virtual sound sources with special attention to the doppler effect." in *Audio Engineering Society Convention 124*, Audio Engineering Society Convention, 2008.

[6] Beig, M., Kapralos, B., Collins, K., and Mirza-Babaei, P., "An introduction to spatial sound rendering in virtual environments and games," *The Computer Games Journal*, 8(3-4), pp. 199–214, 2019, doi: https://doi.org/10.1007/s40869-019-00086-0.

[7] Féron, F.-X., Frissen, I., Boissinot, J., and Guastavino, C., "Upper limits of auditory rotational motion perception," *The Journal of the Acoustical Society of America*, 128(6), pp. 3703–3714, 2010, doi: https://doi.org/10.1121/1.3502456.

[8] Faragher, S., *The Hammond Organ: An introduction to the instrument and the players who made it famous*, Hal Leonard Books, 2011.

[9] Mohammed et al., T. S., "Fault diagnosis of rotating machine based on audio signal recognition system: an efficient approach," *Int. J. Simul. Syst. Sci. Technol,*, 21(1), 2020, doi: https://doi.org/10.5013/IJSSST.a.21.01.08.

[10] Schmele, T. and Lopez, J. J., "Comparisons between VBAP and WFS using Spatial Sound Synthesis," in *Audio Engineering Society Convention 153*, Audio Engineering Society, 2022.

[11] Morse, P. M. and Ingard, K. U., *Theoretical Acoustics*, Princeton University Press, Princeton, New Jersey, 1968.

[12] Berkhout, A. J., "A holographic approach to acoustic control," *Journal of the audio engineering society*, 36(12), pp. 977–995, 1988.

[13] Start, E. W., *Direct sound enhancement by wave field synthesis*, Ph.D. thesis, Technische Universiteit Delft, 1997.

[14] Bleda Pérez, S., *Contribuciones a la implementación de sistemas Wave Field Synthesis*, Ph.D. thesis, Universitat Politècnica de València, 2009, doi: https://doi.org/10.4995/Thesis/10251/6685.

[15] Gerzon, M. A., "Periphony: With-height sound reproduction," *Journal of the audio engineering society*, 21(1), pp. 2–10, 1973.

[16] Daniel, J., *Représentation de champs acoustiques, application à la transmission et à la reproduction de scènes sonores complexes dans un contexte multimédia*, Ph.D. thesis, University of Paris VI, 2000.

[17] Spors, S. and Rabenstein, R., "Spatial aliasing artifacts produced by linear and circular loudspeaker arrays used for wave field synthesis," in *Proceedings of the 120th Audio Engineering Society Convention*, Audio Engineering Society, Paris, France, 2006.

[18] Roads, C., *Computer Music Tutorial*, The MIT Press, Cambridge, MA, USA, 1996.

[19] Torchia, R. H. and Lippe, C., "Techniques for multi-channel real-time spatial distribution using frequency-domain processing," in *Proceedings of the 2004 conference on New Interfaces for Musical Expression (NIME)*, pp. 116–119, Shizuoka University of Art and Culture, Hamamatsu, Japan, 2004, doi: https://doi.org/10.5555/1085884.1085910.

[20] Kim-Boyle, D., "Spectral and Granular Spatialization with Boids," in *Proceedings of the International Computer Music Conference (ICMC)*, pp. 139–142, New Orleans, LA, USA, 2006.

[21] Bates, E., *The Composition and Performance of Spatial Music*, Ph.D. thesis, Trinity College Dublin, Ireland, 2009.

[22] James, S. and Hope, C., "2D and 3D Timbral Spatialisation: Spatial Motion, Immersiveness, and Notions Of space," in *Proceedings of the International Computer Music Conference (ICMC)*, pp. 77–84, Perth, Australia, 2013.